Soft Matter

Seeded laser-induced cavitation for studying high-strain-rate irreversible deformation of soft materials

Journal:	*Soft Matter*
Manuscript ID	SM-ART-04-2020-000710.R2
Article Type:	Paper
Date Submitted by the Author:	06-Aug-2020
Complete List of Authors:	Tiwari, Sacchita; University of Massachusetts Amherst, Mechanical & Industrial Engineering Kazemi-Moridani, Amir; University of Massachusetts Amherst, Mechanical & Industrial Engineering Zheng, Yue; University of California San Diego, Mechanical and Aerospace Engineering Barney, Christopher; University of Massachusetts Amherst McLeod, Kelly; University of Massachusetts Amherst Dougan, Carey; University of Massachusetts Amherst Crosby, Alfred; University of Massachusetts, Polymer Science and Engineering Tew, Gregory; University of Massachusetts, Department of Polymer Science and Engineering Peyton, Shelly; University of Massachusetts Amherst, Chemical Engineering Cai, Shengqiang; UCSD, Department of Mechanical and Aerospace Engineering Lee, Jae-Hwang; University of Massachusetts Amherst, Mechanical & Industrial Engineering

Seeded laser-induced cavitation for studying high-strain-rate irreversible deformation of soft materials

Sacchita Tiwari [a,1], Amir Kazemi-Moridani [a,1], Yue Zheng [b], Christopher W. Barney [c], Kelly R. McLeod [c], Carey E. Dougan[d], Alfred J. Crosby [c], Gregory N. Tew [c], Shelly R. Peyton[d], Shengqiang Cai [b], Jae-Hwang Lee [a,*]

[a] Department of Mechanical and Industrial Engineering, University of Massachusetts, Amherst MA 01003, USA

[b] Department of Mechanical and Aerospace Engineering, University of California at San Diego, La Jolla, CA 9209, USA.

[c] Polymer Science and Engineering Department, University of Massachusetts, Amherst, MA 01003, USA.

[d] Department of Chemical Engineering, University of Massachusetts, Amherst MA 01003, USA

* Corresponding authors:

E-mail address: leejh@umass.edu (J.-H. Lee)

[1] Equal contribution.

Abstract: Characterizing the high-strain-rate and high-strain mechanics of soft materials is critical to understanding the complex behavior of polymers and various dynamic injury mechanisms, including traumatic brain injury. However, their dynamic mechanical deformation under extreme conditions is technically difficult to quantify and often includes irreversible damage. To address such challenges, we investigate an experimental method, which allows quantification of the extreme mechanical properties of soft materials using ultrafast stroboscopic imaging of highly reproducible laser-induced cavitation events. As a reference material, we characterize variably cross-linked polydimethylsiloxane specimens using this method. The consistency of the laser-induced cavitation is achieved through the introduction of laser absorbing seed microspheres. Based on a simplified viscoelastic model, representative high-strain-rate shear moduli and viscosities of the soft specimens are quantified across different degrees of crosslinking. The quantified rheological parameters align well with the time-temperature superposition prediction of dynamic mechanical analysis. The presented method offers significant advantages with regards to quantifying high-strain rate, irreversible mechanical properties of soft materials and tissues, compared to other methods that rely upon the cyclic dynamics of cavitation. These advances are anticipated to aid in the understanding of how damage and injury develop in soft materials and tissues.

1. Introduction

Characterization of tissues and soft materials has been the subject of extensive research over the past few decades.[1–4] Mechanical characterization of soft materials at both macroscopic and microscopic length-scales was possible through modification of existing characterization methods such as tensile/compression tests[5–9], indentation[10–17], nano-indentation[18–21], atomic force microscopy[22–24], and microrheology[25–27], as well as the introduction of novel methods with tailored application to soft matter and biological samples such as needle-induced cavitation[28–30], optical/magnetic tweezers[31–33], elastocapillary bending[34], and confocal rheology.[35] However, nearly all these methods were used to study the low-strain-rate (LSR) responses of soft materials. With all the information available for LSR behaviour of soft materials, there is the increasing need for high-strain-rate (HSR) measurement methods. For instance, quantitative understanding of mechanical effects of blast and impact injuries, such as traumatic brain injury (TBI and mTBI)[36–41] and collateral damage to the surrounding tissue during lithotripsy and laser surgery[42,43] also demands HSR mechanical characterization of various tissues. HSR characterization techniques, such as the Split-Hopkinson pressure bar, have previously been used to study the mechanical responses of soft matter and biological tissue.[44–47] However, these methods may not be ideal for exploring the local properties of soft materials at strain-rates higher than 10^3-10^4 s^{-1} due to the low stiffness and slow wave speeds of soft materials.[48].

Laser-induced cavitation (LIC) is an emerging method, where HSR mechanical responses of soft materials are quantified by observing the oscillatory dynamics of a laser-induced cavity.[49] As seen in the expansion stage of LIC in water,[50] when LIC uses the dielectric breakdown of the medium being investigated, it can suffer from a breakdown instability, which is strongly influenced by unpredictable fluctuation of local physical and chemical properties. Because the fluctuation will inevitably be more severe for actual tissue, which naturally has chemical and physical inhomogeneity, the reliance of LIC on a specimen's dielectric breakdown can lead to less consistent results. Consequently, the utilization of LIC as an HSR characterization tool for heterogeneous biological specimens is limited.

Here, we report a consistent experimental framework for the investigation of HSR responses of soft materials using the initial expansion dynamics. In our seeded laser-induced cavitation (SLIC) approach, laser absorbing microparticles or ablation seeds are introduced within the test medium to generate a laser-induced cavity. Through ablation of a single seed using a laser pulse, high-pressure gases in the medium result in the expansion of the initial cavity and the expansion dynamics are recorded using a synchronized ultrafast stroboscopic imaging technique. Instead of ablating a specimen of unknown nonlinear optical characteristic in LIC, ablation seeds of known laser absorption are used in SLIC. Since the nonlinear ablation process is de-coupled from the specimen's unpredictable optical nonlinearity, more predictable cavitation is possible. Moreover, in conventional LIC, because the ablation volume and position are primarily determined by the ellipsoidal voxel of a focused laser beam at the focal point, a cavity generated at the focal point in

LIC has limited tunability of cavitation. In contrast, the location and geometry of cavity can be precisely controlled in SLIC by positioning a shaped seed (rod-like or curved) at a specific location in a specimen. This geometrical tunability and positional flexibility of SLIC can make it more diverse and flexible characterization method. Note that SLIC is distinct from needle-induced cavitation (NIC) in terms of accessible range of strain rate and delivery of cavitation energy (directly delivered via pressurized fluid in NIC and remotely delivered via optical waves in SLIC). More comprehensive comparisons between various cavitation techniques are well described in a recent perspective.[49]

This SLIC approach enables us to quantitatively probe the initial expansion dynamics of cavitation at a high spatial and temporal resolution. Estrada *et al.* introduced an approach for the HSR characterization of soft materials based on conventional LIC.[51] Despite this LIC method demonstrating important progress in the study of the HSR behaviour of soft materials, the regular oscillatory motion of a cavity may not always be possible, especially when a cavitation-to-fracture transition exists during the initial expansion stage of LIC (for example, see **Fig. 1**).[52,53] Therefore, a LIC-based characterization method using the initial expansion stage of cavity dynamics should be developed to assess the intrinsic HSR properties of a soft material, while minimizing challenges arising from a complex ablation process, short time scale, and overwhelming inertial effect.

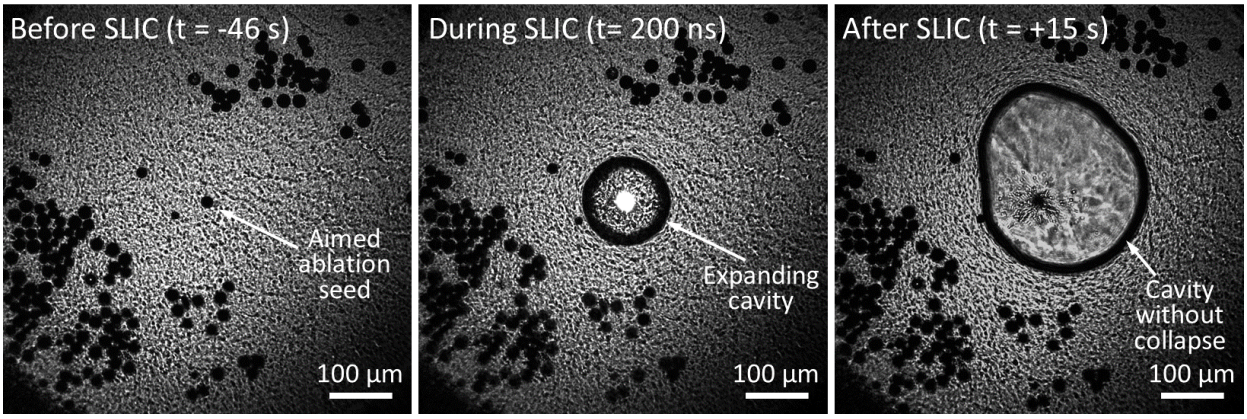

Figure 1 Unconventional cavitation behavior observed from SLIC of a mouse brain slice. The consecutive micrographs show the irreversible deformation of the brain tissue, for which the expansion-stage cavitation rheology may be necessary.

2. Experimental method

2.1 Construction of the optical system

Black paramagnetic polyethylene microspheres (Cospheric LLC) were used as the ablation seeds without any modification. The necessary intensity for ablation of the seed was well below the dielectric breakdown threshold of the medium due to the high optical absorption of the seeds. **Fig. 2a** illustrates the optical system of SLIC near a sample stage. An ablation laser pulse (pulse

duration ~7 ns, wavelength 1064 nm) was generated from a Nd:YAG pulsed laser (INDI-40-10, Spectra-Physics) using an external trigger. Moreover, to lower the laser intensity at the ablation seed to below the dielectric breakdown intensity, the focal point of the laser pulse was adjusted to be approximately 1 mm behind the ablation seed. After delivering the ablation laser pulse to the seed, a continuous train of ultrafast light pulses (wavelength ~780 nm) generated by a Ti:Sapphire oscillator (repetition rate ~80 MHz; Mai-Tai HP, Spectra-Physics), were gated by a series of electro-optical modulators to illuminate the SLIC event. The delay time between the ablation laser pulse and the first imaging pulse is T_1 and the time difference between adjacent imaging pulses is T_2. In the SLIC image in **Fig. 2b**, for example, T_1 and T_2 were 145.0 ns and 478.6 ns, respectively. Thus, $t_1 = T_1 = 145$ ns, $t_2 = T_1 + T_2 = 624$ ns, $t_3 = T_1 + 2T_2 = 1102$ ns, and so on. As an individual pulse duration of the illumination light is less than 100 fs, this exposure time can virtually eliminate any motion blurring. A narrow bandpass filter for 780 nm (Semlock) was used to reject background light noise originating from the light flash during the ablation of the seed. The distance between the ablation seed and the objective lens was kept constant using a live image of the system without the need for any further alignment of the ablation beam. A radius of the compressional wave front, R_s is shown in **Fig. 2b**. The speed of the compressional wave, v_s is 1,517 m/s, and is very close to the calculated compressional wave speed, 1,506 m/s, given by $\sqrt{K/\rho}$, where K (2.2 GPa)[54] and ρ (970 kg/m^3)[55] are the bulk modulus and mass density of PDMS respectively.

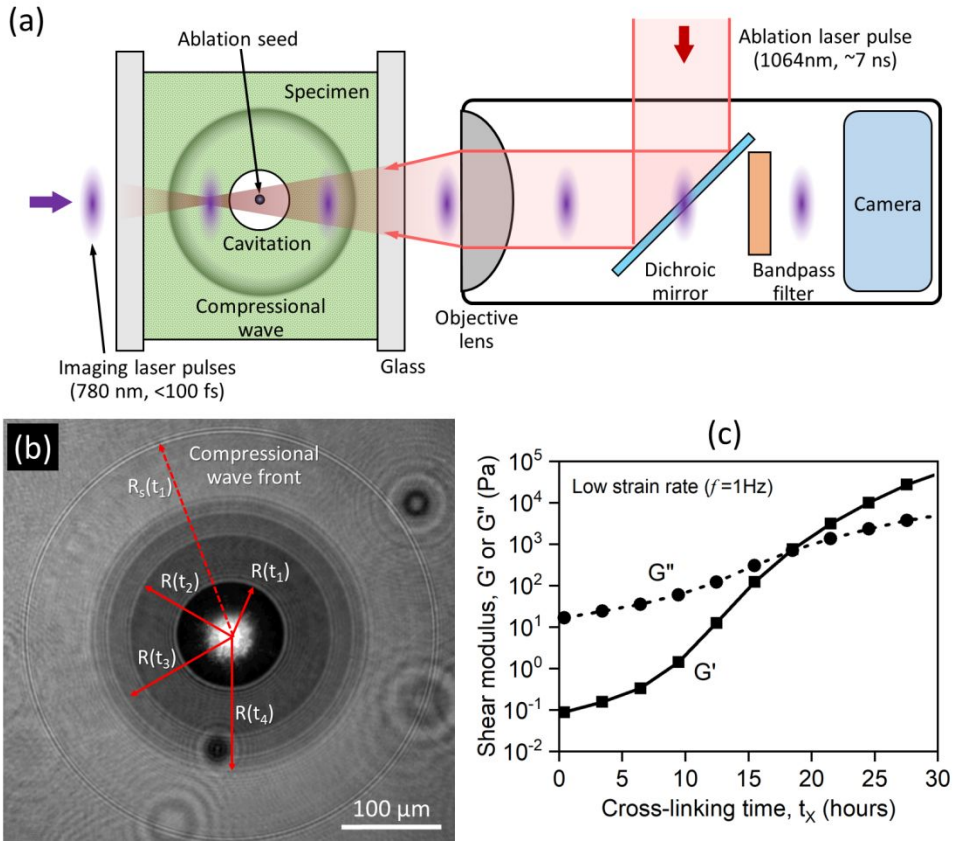

Figure 2 SLIC characterization and an example of application. (a) Schematic illustration of the SLIC experimental setup. **(b)** An example of an ultrafast micrograph of an expanding laser-induced cavity, taken by four illumination pulses. **(c)** Viscoelastic characteristics of PDMS at 1 Hz for varying crosslinking time.

2.2 Model soft material system

A thermally crosslink-able polydimethylsiloxane (PDMS) elastomer kit (Sylgard 184®, Dow Chemical) was used as a model soft material system, where its viscoelastic properties vary with the crosslinking reaction time (t_X) at the room temperature (21 °C). After mixing the base and the crosslinking agent of the polymer system at a weight ratio of 10:1, the ablation seeds were added to the mixture and stirred for about 5 minutes to achieve a homogenized distribution of the seeds throughout the entire mixture. After degassing the mixture for under 10 minutes, a 2 mm thick container with two sides made of glass coverslips (Fisherbrand™, 25 mm × 25 mm × 0.15 mm) and edges sealed using a generic hot glue was prepared. The mixture was subsequently poured in the container and the experiments were performed after crosslinking progressed at the room temperature. For uncrosslinked PDMS samples, the ablation seeds were observed to continuously sink to the bottom of the sample container due to their heavier density than that of PDMS. To suppress the gravitation effect on the ablation seeds, the condition of t_X was 5 h was selected as the shortest crosslinking time.

2.3 Low-strain-rate rheology

A significant advantage of SLIC is the ability to compare HSR and conventional LSR mechanical properties, in order to learn about material property transitions associated with high-rate loading. To quantify the LSR properties of the PDMS specimens, conventional parallel plate rheometric characterization was performed (AR 2000, TA Instruments). Data was collected every 3 hours for 30 hours of t_X at the room temperature. Measured storage shear (G') and loss shear (G'') modulus at f = 1 Hz are shown in **Fig. 2c**. As G' became larger than G'' after t_X=18 h, it shows that the PDMS underwent a continuous transition from viscous liquid to viscoelastic solid within the crosslinking window of 24 h. The LSR dynamic viscosity at 1 Hz, given by $\mu_{LSR} = G''/\omega$, increased substantially from 5 Pa ·s (t_X=5 h) to 320 Pa ·s (t_X=24 h). Frequency-dependent (0.1 – 100 Hz) storage elongation moduli (E') of PDMS for $t_X = 24$ h were measured using dynamic mechanical analysis (DMA) with a compression clamp (a radius of 7.5 mm) at three different temperatures (20, -20, and -40 °C). For the clamping geometry, the measured E' was shifted using a bonded interface correction factor originally developed by Gent.[56] Based on time-temperature superposition principle , the two low-temperature moduli curves were shifted toward higher frequency ranges by the Williams-Landel-Ferry (WLF) equation[57] with a reference temperature of 20 °C.

2.3 Estimation of the temperature rise and calibration of SLIC

Since the mechanical characteristics of soft polymer systems can be highly temperature-dependent, one might expect that the laser-induced hot gases in SLIC to alter the dynamics of cavitation. However, the quantification of local temperatures near a rapidly expanding cavity is technically challenging due to the small temporal scale. To estimate any noticeable rise from the hot gases, sub-100μm size flakes of crystalline eicosane, a short chain linear alkane (Sigma-Aldrich), were added when preparing the PDMS specimens. Since the melting temperature of eicosane is near the room temperature (T_m= 36 – 38 °C[58] at atmospheric pressure), the eicosane flakes dispersed in the PDMS specimen can serve as a temperature reference to estimate local temperature rise. Cavitation in the vicinity of the flakes was used to estimate temperature rise close to the cavity (**Fig. 3a**). During the expansion of a cavity, although some of the flakes were very close to the boundary of the cavity, no sign of melting was observed (**Fig. 3b**). This result was also confirmed by the post-cavitation image (**Fig. 3c**). Upon closer observation, as seen in **Fig. 3d** & **3e**, the original small flake was rotated but did not show any noticeable signs of melting. This finding suggests that the temperature rise in the medium was insignificant due to low thermal diffusivity of the polymeric specimen and short time scale (< 10 μs).

Under a fixed optical alignment, the initial state of the SLIC process was primarily determined by a diameter of the seed and energy of the ablation laser pulse. Therefore, we can define the initial state of the cavitation as the end of the seed ablation process that happens over the temporal width of the ablation laser pulse. **Fig. 3f** shows that the maximum radius (R_{max}) of a cavitation event can be systematically controlled by altering either the ablation seed diameter or the laser pulse energy. Note that the actual laser pulse energy absorbed by the seed was significantly lower than the total laser energy since the ablation beam diameter near the seed was larger than the diameter of the seed (as depicted in **Fig. 2a**). The effect of seed size appeared to be linear for the range of seed diameters studied (11 – 23 μm) and was less profound compared to the ablation energy effect. Variability in the data most likely originates from the fluctuation of the ablation laser output. The plot demonstrates that SLIC is a stable and consistent characterization method, capable of quantifying the HSR mechanical response. By performing the SLIC experiments as the PDMS crosslinking reaction progressed, all defining parameters of the sample independent of crosslink density remained constant during the experiment. For instance, as seen in **Fig. 3f**, since the size of a seed and the ablation energy alter the initial conditions of SLIC, ablation seeds within a narrow range of diameters (20 – 22 μm) were used, which is depicted as a grey region in **Fig. 3f**. Additionally, the ablation laser energy was fixed at 73 μJ to ensure a complete view of all cavities without changing the optical field of view of the imaging system.

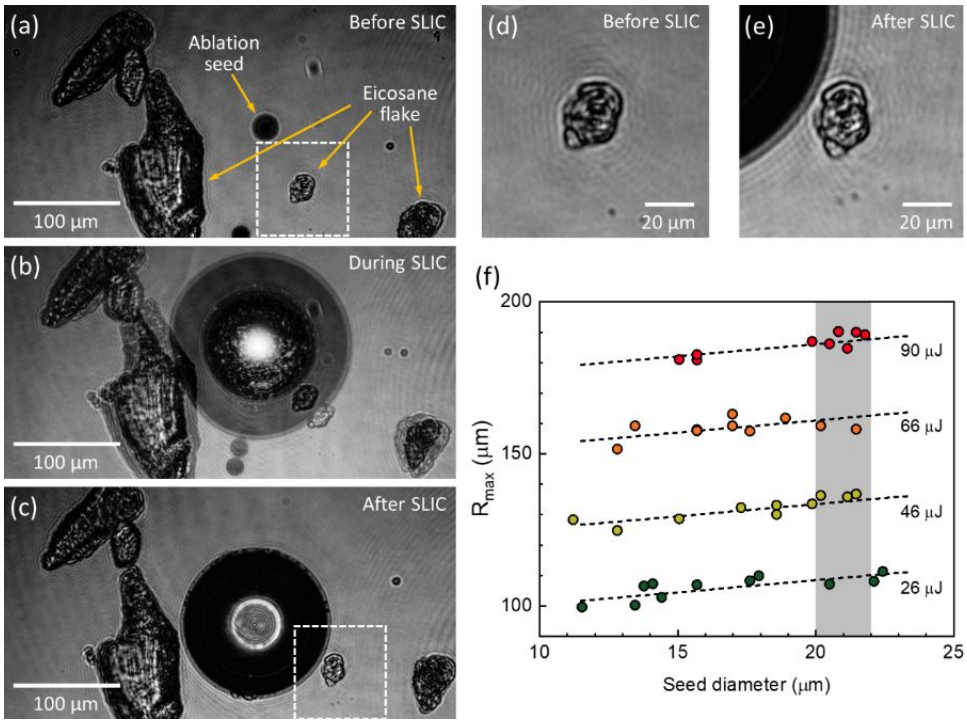

Figure 3 Experimental characteristics of SLIC. **(a)** Eicosane flakes dispersed around an ablation seed in PDMS before SLIC. **(b)** A double-exposed image during SLIC shows cavity motion and radial displacement of the flakes. **(c)** A residual cavity and the displaced flakes after SLIC. Magnified views of a small eicosane flake **(d)** before and **(e)** after SLIC show rotated but almost identical features. **(f)** Maximum cavity radius is systematically altered by controlling the ablation seed and laser pulse energy. For the SLIC characterization, the ablation seeds within the grey range were used.

3. Results and discussion

For different crosslinking time t_X, the mass density (ρ) is approximately constant and all the differences during SLIC are assumed to originate from the material parameters associated with time-varying crosslinking network of PDMS. **Fig. 4** shows measured instantaneous radii of an expanding and collapsing cavity, $R(t)$, for PDMS samples, crosslinked for 5, 12, 20, and 24 hours at the room temperature. Note that 11 to 16 independent SLIC events were used to demonstrate statistical trends of the cavity dynamics for each case of crosslinking time. $R(t)$ reaches $R_{\max}$ at $t = t_{\max}$. While $R_{\max}$ and $t_{\max}$ monotonically decrease for a longer t_X, the overall trend of cavity expansion is similar for all t_X because the early time HSR cavity expansion dynamics of a soft material is primarily governed by inertia (or mass density) of the material. During the contraction stage (after reaching $R_{\max}$), the contraction speed increases as t_X increases (except $t_X = 24h$). The exceptional trend observed at $t_X = 24h$ may indicate that the elastically stored energy was additionally dissipated through cavity-induced fractures. For the cases in which the contraction dynamics can be affected by cavity-induced damage, the mechanical characterization method

presented here, which only relies upon cavitation dynamics during the expansion stage, is certainly preferred.

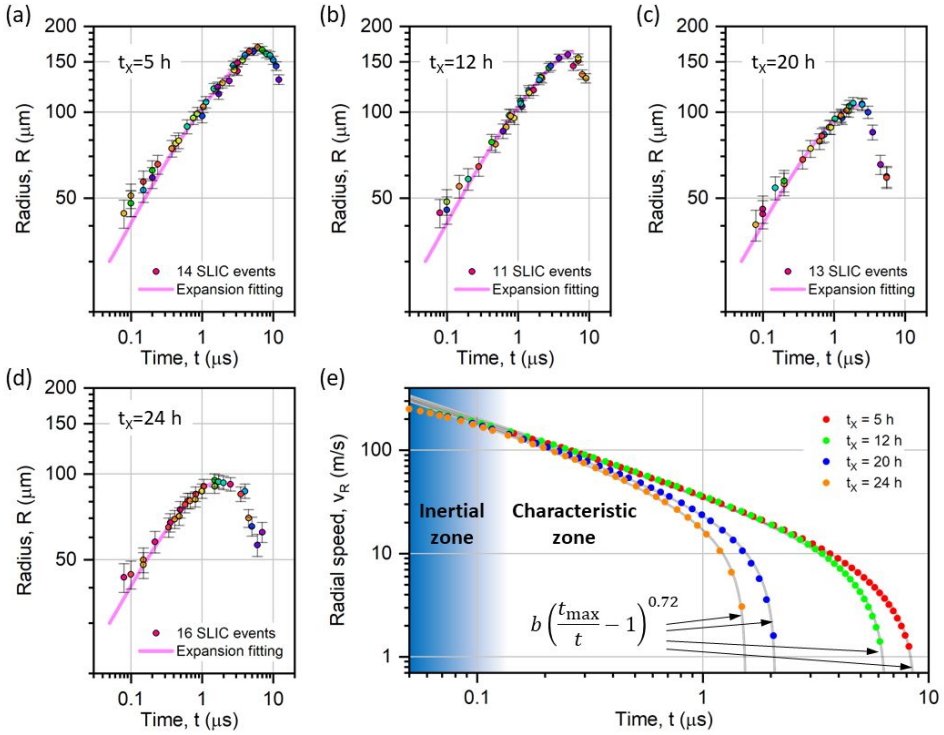

Figure 4 SLIC experimental results and model-based fitting. (a)-(d) Instantaneous cavity radii for the samples prepared with four cross-linking times are shown with fitting curves of radius and radial velocity. The y-error bars are approximately 5 μm due to the fluctuation of the ablation laser shown in Fig. 3f while a negligible temporal error (< 1 ps) is not displayed. The different filled in colors of the circular symbols represent different SLIC events. **(e)** Radial speeds are shown for the four different cross-linking times of PDMS. Other than within the inertial regime, the trends of expansion speeds are described by a single form of equation.

The cavitation dynamics were modelled by continuum mechanics based on the Kelvin-Voigt viscoelastic model, which is the simplest viscoelasticity model, involving only two fitting parameters. Although various models with a range of rheological parameters can be considered when modelling cavity dynamics, the difference between the models tends to be insignificant[59] within a single expansion or contraction stage. Moreover, we intended from the beginning to use simple models with less material parameters to focus on the main physics of the SLIC experiments. Our preference for simple models is also related to the fact that the HSR cavity dynamics of soft materials is overwhelmingly dependent on a material's inertia (or mass density). Thus, our model based on essential viscoelastic parameters is optimally suited for the presented SLIC-based rheological characterization using the initial expansion dynamics. We assumed that the cavity in the material was a spherical void in an infinite medium and the surface energy was negligible. Taking the surrounding material as an incompressible viscoelastic solid with finite deformation, the following equation for studying the dynamic behaviour of cavitation has been developed.[60]

$$\frac{p-p_\infty}{\rho} = R\frac{d^2R}{dt^2} + \frac{3}{2}\left(\frac{dR}{dt}\right)^2 + \frac{4\mu dR}{R\ dt} + \frac{G}{\rho}\left[\frac{5}{2} - 2\left(\frac{R}{R_0}\right)^{-1} - \frac{1}{2}\left(\frac{R}{R_0}\right)^{-4}\right] \quad (1)$$

where p is the instantaneous pressure inside the cavity and p_∞ is the ambient pressure. The first two terms on the right hand side describe the inertial behavior, while the 3rd term and the bracketed term represent viscosity and neo-Hookean elasticity of the medium, respectively. The material's mass density ρ was measured independently and assumed to be constant during the SLIC process. The two fitting parameters, G and μ, for the spring and dashpot were interpreted as a cavitation-based shear modulus and viscosity, which represented the HSR properties of the specimen. The initial cavity radius was denoted as R_0, which was given by the radius of the ablation seed (~10 μm). Eq. (1) can be reduced to the Rayleigh-Plesset equation of bubble dynamics in fluid by neglecting the last elasticity term.

The gases inside the cavity were assumed to behave as an ideal gas with homogeneous pressure undergoing adiabatic expansion process:

$$pR^{3\gamma} = p_0R_0^{3\gamma} = k \quad (2)$$

where γ, p_0, and k are the adiabatic index, the initial pressure, and a constant, respectively. Any phase transitions of the gases, such as condensation, are not considered during the expansion process due to the lack of water, the short time scale of the expansion event (< 10 μs), and the intrinsically low thermal diffusivity of PDMS. Moreover, because gases produced by the laser ablation were an unidentified gas mixture, we assumed 7/5 (diatomic gases) for the index. The constant k has to be determined using p_0, which can be estimated using Eq. (2). In the SLIC experiments, the very early trend of $R(t)$ was indistinguishable, regardless of t_X. This similarity in response for $t < 50$ ns for networks of different crosslinking extent is understood by the initial conditions, $\lim_{t\to 0} R = R_0$, $\lim_{t\to 0} \dot{R} = 0$, and negligible elastic strain. Therefore, we estimated p_0 in Eq. (1) by measuring a radial speed, $v_R = dR/dt$, and a radial acceleration, d^2R/dt^2 while neglecting both viscous and elastic terms for $t < 50$ ns. The initial pressure estimate provided a value of approximately 90 MPa.

The results of the material's cavity radius and velocity, which were fitted by solving the ordinary differential equation, Eq. (1), are shown in **Fig. 4a-d**. For the fitting of expansion dynamics, the data points from the expansion stage ($R(t) \le R_{MAX}(t_{max})$) were used. Using the viscoelastic fitting curves of $R(t)$ without the contraction data, $v_R(t)$ was calculated (**Fig. 4e**). Except in the early stage ($t < 150$ ns), $v_R(t)$ in the expansion stage ($t \le t_{max}$) can be accurately expressed by an empirical equation:

$$v_R(t) = b\left(\frac{t_{max}}{t} - 1\right)^\alpha, \quad (3)$$

where the exponent, α is 0.72 ($\sim 1/\sqrt{2}$) for the four cases, and b is a constant (7.8, 10.2, 21.5, and 26.0 m/s for t_X= 5, 12, 20, and 24 h, respectively). The single exponent implies that the cavity

dynamics are governed by identical HSR viscoelasticity physics for $t > 150$ ns. The early stage of expansion ($t < 150$ ns) is very similar, regardless of t_X, mainly due to the dominant role of inertia; this can be regarded as the 'inertial zone,' while the rest of expansion can be regarded as the 'characteristic zone,' in which material's properties can be quantified.

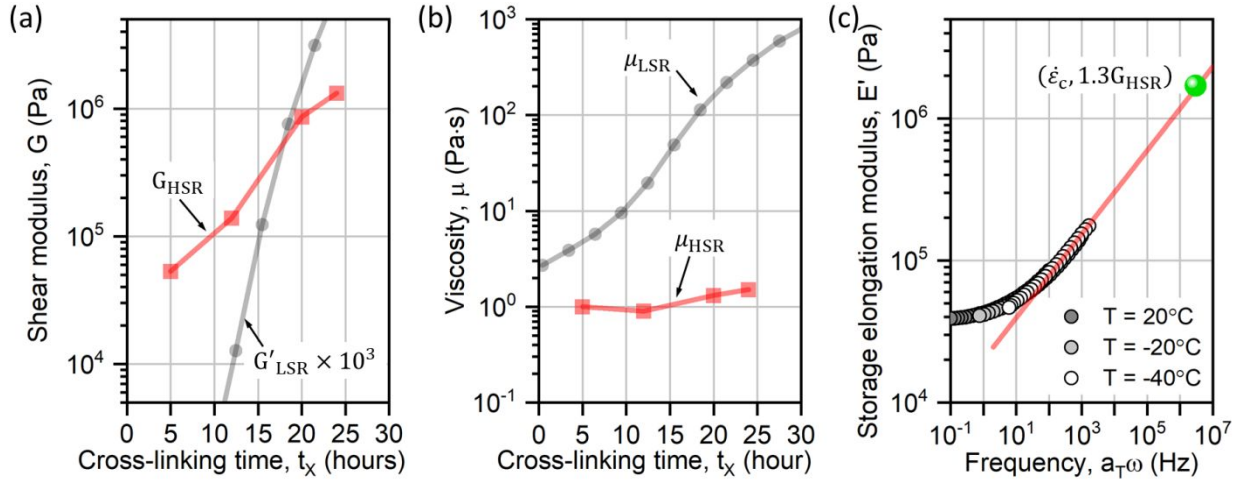

Figure 5 Comparison of LSR and HSR viscoelastic characteristics. (a) Cavitation-based HSR shear modulus and **(b)** HSR viscosity of PDMS depending on the crosslinking time are quantified by the model-based fitting. For comparison, the LSR storage shear modulus and viscosity at 1 Hz are plotted, where the original storage shear modulus is shifted by 10^3 for better display. **(c)** A master curve of frequency-dependent storage Young's moduli of PDMS from the oscillatory measurements is extrapolated for high frequency dynamics where the green symbol shows the cavitation-based modulus and the circumferential strain rate at the boundary of the inertial regime.

Using the fitting parameters, G_{HSR} and μ_{HSR}, measured by SLIC, we directly compare the mechanical properties of the different PDMS networks at HSRs from SLIC to those measured by conventional dynamic mechanical analysis at low strain rates (LSRs) (**Fig. 5a-5b**). The direct comparison of the HSR and LSR shear modulus and viscosity as a function of t_X indicates two important characteristics. First, the HSR materials' parameter changes are significantly less sensitive to t_X, as compared to the LSR parameters, primarily because the larger chain length scales, such as the network architecture, are changing as a function of crosslinking time while the local segmental dynamics, which are more relevant to the HSR responses, are not changing. Second, G_{HSR} is several orders higher than G'_{LSR} due to substantial strain-rate hardening. The varying range of G_{HSR} for the different networks is wide enough to provide a sufficient resolution in the HSR characterization of soft materials. Third, μ_{HSR} was significantly lower than μ_{LSR} with a weak dependency on the crosslinking. This decrease in μ indicates that the dissipative mechanisms, associated with the viscosity contribution, are less crucial in SLIC. It is worthy to mention the possibility of cavity-induced damage although we did not explicitly confirm any such damage in this report. Smaller scale voids or damage, below the optical resolution of our SLIC imaging system, may affect the viscoelastic parameters of the specimens[61] determined from the measured cavity dynamics.

Beyond these direct comparisons that give insight into segmental and chain responses, it is also interesting to investigate possible quantitative connections between HSR and LSR materials parameters. To enable this comparison, we first estimate the circumferential strain rate of a specimen near the boundary of an expanding cavity can be estimated by $\dot{\varepsilon}_c = v_R/R$, which is approximately $3 \times 10^6 s^{-1}$ at the onset of the characteristic zone. With this estimate of the strain rate, we plot the storage elongational modulus, E' as a function of shifted frequency. **Fig. 5c** shows the master curve of the frequency-dependent E' of PDMS ($t_X = 24$ h), horizontally shifted by the WLF equation, and power-law extrapolation to predict E' at HSR. Surprisingly, $E' \cong 1.3 G_{HSR}$ (1.7 MPa) from the SLIC and $\dot{\varepsilon}_c$ ($3 \times 10^6 s^{-1}$) are quantitatively consistent with the extrapolated trend. This finding suggests that the dynamics of storing mechanical energy for this PDMS material at the segmental and network scales are simply connected by a power law. Note that generally, polymers tend to approach a plateau modulus at high frequencies, where dynamics are faster than segmental motions associated with a given polymer architecture .[62] For PDMS, this glassy plateau is observed at temperatures near and below approximately -125 °C, where the storage modulus have been measured to be approximately 4 GPa.[63] The HSR moduli extracted from SLIC (**Fig. 5c**) are more than three orders of magnitude less, suggesting that the cavitation dynamics are significantly slower than the segmental dynamics of the highly flexible PDMS chains. SLIC with polymer networks with slower segmental dynamics will provide more insight into correlations between cavitation dynamics and molecular motion. Furthermore, using the photoelastic effect,[64] we can envision detection of the strain-rate-induced glassy state of a polymer via a temperature-controlled SLIC system with polarimetric imaging optics.

4. Conclusions

We demonstrate the SLIC method as an effective framework to quantify the HSR mechanical characteristics of soft materials by introducing the ablation seeds for more predictable and consistent laser ablation conditions. Using a controlled soft material system whose cross-linking density can be selectively varied, the contribution of the network connectivity to the HSR viscoelastic properties is quantified by the SLIC method. Based on the Kelvin-Voigt viscoelastic model, HSR viscosity and shear modulus are quantified with respect to the varying cross-linking density at the representative strain rate of 3×10^6 s^{-1}. The HSR elastic modulus from the SLIC method shows exceptionally good agreement with the extrapolated LSR elastic modulus based on the time-temperature superposition principle. If this finding is generalized to other polymer networks, it will provide a powerful method for understanding and predicting HSR failure processes in these materials that are widely-used in a range of applications, including medical technologies and systems for extreme environments. Furthermore, as HSR rheological characterization is possible using the initial expansion dynamics of cavitation, this SLIC method will particularly be useful in studying HSR physical response of various soft tissues including brains.

Acknowledgements

This research was supported by the Office of Naval Research under grant N00014-17-1-2056.

Author Contributions

S.T., A.K.-M., J.-H.L. (development of seeded laser-induced cavitation, cavitation experiments, writing the original manuscript, analysis); Y.Z., S.C. (numerical modeling, fitting, analysis); C.W.B, A.J.C. (dynamic mechanical analysis, low-strain-rate rheology, analysis); K.R.M., G.N.T. (polymer preparation, analysis); S.T, C.E.D, S.R.P. (brain tissue preparation, cavitation experiments). All authors reviewed and edited later versions.

References

[1] D. T. N. Chen, Q. Wen, P. A. Janmey, J. C. Crocker, A. G. Yodh, *Annu. Rev. Condens. Matter Phys.* **2010**, *1*, 301.

[2] S. Zörner, M. Kaltenbacher, R. Lerch, A. Sutor, M. Döllinger, *J. Biomech.* **2010**, *43*, 1540.

[3] P. Cicuta, A. M. Donald, *Soft Matter* **2007**, *3*, 1449.

[4] R. Akhtar, M. J. Sherratt, J. K. Cruickshank, B. Derby, *Mater. Today* **2011**, *14*, 96.

[5] E. C. Muniz, G. Geuskens, *Macromolecules* **2001**, *34*, 4480.

[6] S. P. Marra, K. T. Ramesh, A. S. Douglas, *Mater. Sci. Eng. C* **2001**, *14*, 25.

[7] B. . Johnson, D. . Beebe, W. . Crone, *Mater. Sci. Eng. C* **2004**, *24*, 575.

[8] X. Zhao, N. Huebsch, D. J. Mooney, Z. Suo, *J. Appl. Phys.* **2010**, *107*, 063509.

[9] J.-H. Kim, A. Nizami, Y. Hwangbo, B. Jang, H.-J. Lee, C.-S. Woo, S. Hyun, T.-S. Kim, *Nat. Commun.* **2013**, *4*, 1.

[10] G. Constantinides, Z. I. Kalcioglu, M. McFarland, J. F. Smith, K. J. Van Vliet, *J. Biomech.* **2008**, *41*, 3285.

[11] I. Levental, K. R. Levental, E. A. Klein, R. Assoian, R. T. Miller, R. G. Wells, P. A. Janmey, *J. Phys. Condens. Matter* **2010**, *22*, 194120.

[12] Y. Hu, X. Zhao, J. J. Vlassak, Z. Suo, *Appl. Phys. Lett.* **2010**, *96*, 121904.

[13] Z. I. Kalcioglu, M. Qu, K. E. Strawhecker, T. Shazly, E. Edelman, M. R. VanLandingham, J. F. Smith, K. J. Van Vliet, *Philos. Mag.* **2011**, *91*, 1339.

[14] S. J. Lee, J. Sun, J. J. Flint, S. Guo, H. K. Xie, M. A. King, M. Sarntinoranont, *J. Biomed. Mater. Res. Part B Appl. Biomater.* **2011**, *97B*, 84.

[15] Y. Hu, J.-O. You, D. T. Auguste, Z. Suo, J. J. Vlassak, *J. Mater. Res.* **2012**, *27*, 152.

[16] B. G. Bush, J. M. Shapiro, F. W. DelRio, R. F. Cook, M. L. Oyen, *Soft Matter* **2015**, *11*, 7191.

[17] J. Delavoipière, Y. Tran, E. Verneuil, A. Chateauminois, *Soft Matter* **2016**, *12*, 8049.

[18] D. M. Ebenstein, L. A. Pruitt, *J. Biomed. Mater. Res.* **2004**, *69A*, 222.

[19] J. D. Kaufman, G. J. Miller, E. F. Morgan, C. M. Klapperich, *J. Mater. Res.* **2008**, *23*, 1472.

[20] P. O. Guglielmi, E. G. Herbert, L. Tartivel, M. Behl, A. Lendlein, N. Huber, E. T. Lilleodden, *J. Mech. Behav. Biomed. Mater.* **2015**, *46*, 1.

[21] C. T. McKee, J. A. Last, P. Russell, C. J. Murphy, *Tissue Eng. Part B Rev.* **2011**, *17*, 155.

[22] T. R. Matzelle, G. Geuskens, N. Kruse, *Macromolecules* **2003**, *36*, 2926.

[23] Z. Drira, V. K. Yadavalli, *J. Mech. Behav. Biomed. Mater.* **2013**, *18*, 20.

[24] J. I. Kilpatrick, I. Revenko, B. J. Rodriguez, *Adv. Healthc. Mater.* **2015**, *4*, 2456.

[25] A. I. Van Den Bulcke, B. Bogdanov, N. De Rooze, E. H. Schacht, M. Cornelissen, H. Berghmans, *Biomacromolecules* **2000**, *1*, 31.

[26] F. Del Giudice, M. Tassieri, C. Oelschlaeger, A. Q. Shen, *Macromolecules* **2017**, *50*, 2951.

[27] W. Liu, C. Wu, *Macromol. Chem. Phys.* **2018**, *219*, 1700307.

[28] J. A. Zimberlin, N. Sanabria-DeLong, G. N. Tew, A. J. Crosby, *Soft Matter* **2007**, *3*, 763.

[29] S. Kundu, A. J. Crosby, *Soft Matter* **2009**, *5*, 3963.

[30] C. W. Barney, Y. Zheng, S. Wu, S. Cai, A. J. Crosby, *Soft Matter* **2019**, *15*, 7390.

[31] K. Svoboda, S. M. Block, *Annu. Rev. Biophys. Biomol. Struct.* **1994**, *23*, 247.

[32] P. Kollmannsberger, B. Fabry, *Rev. Sci. Instrum.* **2007**, *78*, 114301.

[33] A. Pommella, V. Preziosi, S. Caserta, J. M. Cooper, S. Guido, M. Tassieri, *Langmuir* **2013**, *29*, 9224.

[34] J. Bae, T. Ouchi, R. C. Hayward, *ACS Appl. Mater. Interfaces* **2015**, *7*, 14734.

[35] S. K. Dutta, A. Mbi, R. C. Arevalo, D. L. Blair, *Rev. Sci. Instrum.* **2013**, *84*, 063702.

[36] V. E. Johnson, W. Stewart, D. H. Smith, *Exp. Neurol.* **2013**, *246*, 35.

[37] D. Kilinc, G. Gallo, K. A. Barbee, *Exp. Neurol.* **2008**, *212*, 422.

[38] J. D. Morse, J. A. Franck, B. J. Wilcox, J. J. Crisco, C. Franck, *Ann. Biomed. Eng.* **2014**, *42*, 2501.

[39] D. F. Meaney, D. H. Smith, *Clin. Sports Med.* **2011**, *30*, 19.

[40] M. K. Nyein, A. M. Jason, L. Yu, C. M. Pita, J. D. Joannopoulos, D. F. Moore, R. A. Radovitzky, *Proc. Natl. Acad. Sci. U. S. A.* **2010**, *107*, 20703.

[41] A. Ramasamy, A. M. Hill, S. Masouros, I. Gibb, A. M. J. Bull, J. C. Clasper, *J. R. Soc. Interface* **2011**, *8*, 689.

[42] A. Vogel, *Phys. Med. Biol.* **1997**, *42*, 895.

[43] A. Vogel, P. Schweiger, A. Frieser, M. N. Asiyo, R. Birngruber, *IEEE J. Quantum*

Electron. **1990**, *26*, 2240.

[44] B. Song, W. Chen, *Exp. Mech.* **2004**, *44*, 622.

[45] B. Song, W. Chen, *Exp. Mech.* **2004**, *44*, 300.

[46] B. Song, W. Chen, Y. Ge, T. Weerasooriya, *J. Biomech.* **2007**, *40*, 2999.

[47] F. Pervin, W. W. Chen, *J. Biomech.* **2009**, *42*, 731.

[48] W. Chen, B. Song, *Split Hopkinson (Kolsky) Bar*, Springer US, Boston, MA, **2011**.

[49] C. W. Barney, C. E. Dougan, K. R. McLeod, A. Kazemi-Moridani, Y. Zheng, Z. Ye, S. Tiwari, I. Sacligil, R. A. Riggleman, S. Cai, J.-H. Lee, S. R. Peyton, G. N. Tew, A. J. Crosby, *Proc. Natl. Acad. Sci.* **2020**, *117*, 9157.

[50] A. Vogel, S. Busch, U. Parlitz, *J. Acoust. Soc. Am.* **1996**, *100*, 148.

[51] J. B. Estrada, C. Barajas, D. L. Henann, E. Johnsen, C. Franck, *J. Mech. Phys. Solids* **2018**, *112*, 291.

[52] S. B. Hutchens, S. Fakhouri, A. J. Crosby, *Soft Matter* **2016**, *12*, 2557.

[53] J. Kang, C. Wang, S. Cai, *Soft Matter* **2017**, *13*, 6372.

[54] I. D. Johnston, D. K. McCluskey, C. K. L. Tan, M. C. Tracey, *J. Micromechanics Microengineering* **2014**, *24*, 035017.

[55] S. Sakarya, G. Vdovin, P. M. Sarro, *Sensors Actuators A Phys.* **2003**, *108*, 271.

[56] A. N. Gent, E. A. Meinecke, *Polym. Eng. Sci.* **1970**, *10*, 48.

[57] M. L. Williams, R. F. Landel, J. D. Ferry, *Am. Chem. Soc.* **1955**, *77*, 3701.

[58] A. Genovese, G. Amarasinghe, M. Glewis, D. Mainwaring, R. A. Shanks, *Thermochim. Acta* **2006**, *443*, 235.

[59] B. Dollet, P. Marmottant, V. Garbin, *Annu. Rev. Fluid Mech.* **2019**, *51*, 331.

[60] R. Gaudron, M. T. Warnez, E. Johnsen, *J. Fluid Mech.* **2015**, *766*, 54.

[61] R. M. Elder, D. B. Knorr, J. W. Andzelm, J. L. Lenhart, T. W. Sirk, *Soft Matter* **2016**, *12*, 4418.

[62] V. V. Palyulin, C. Ness, R. Milkus, R. M. Elder, T. W. Sirk, A. Zaccone, *Soft Matter* **2018**, *14*, 8475.

[63] N. Bosq, N. Guigo, J. Persello, N. Sbirrazzuoli, *Phys. Chem. Chem. Phys.* **2014**, *16*, 7830.

[64] L. R. G. Treloar, *Trans. Faraday Soc.* **1954**, *50*, 881.

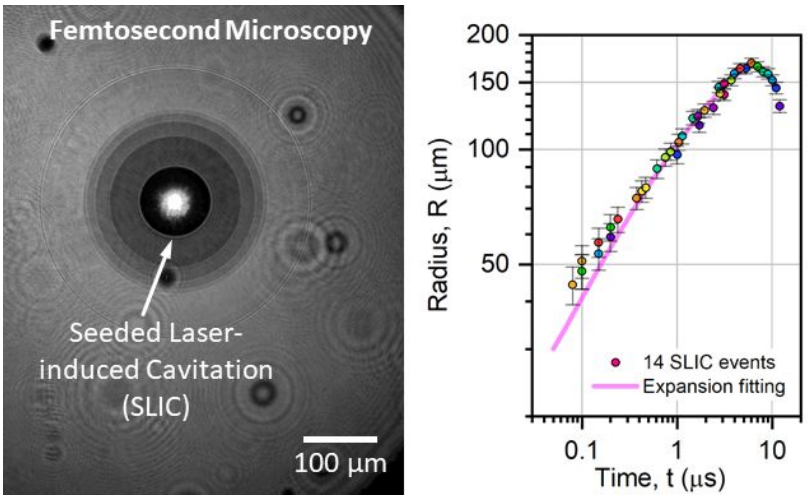

High-strain-rate rheological properties of soft materials are quantified by the observation of a rapidly expanding microscopic cavity.